

Potential for the discovery of the protophobic boson at the STCF

Althaf M. *¹ and Triparno Bandyopadhyay †¹

¹Department of Physics and Nanotechnology, College of Engineering and Technology, SRM Institute of Science and Technology, SRM Nagar, Kattankulathur, Tamil Nadu 603203.

December 18, 2025

Abstract: We study the morphology of the main drift chamber (MDC) to be built around the collision point of the proposed Super tau-charm facility (STCF), to check for its suitability in discovering the 17 MeV protophobic boson (X17 boson), hypothesised as a solution to the persistent ATOMKI nuclear-transition anomalies. These anomalies, observed in the excited ${}^8\text{Be}$, ${}^4\text{He}$, ${}^{12}\text{C}$, ${}^{16}\text{O}$ nuclear transitions, have been interpreted as evidence for a \sim 17 MeV, protophobic vector boson. Using the TrackEff framework, we perform detector-level simulations of the STCF MDC, and evaluate displaced-vertex sensitivities towards the protophobic boson, across the relevant mass-coupling parameter space. We study benchmark scenarios with visible and dark decay channels to perform likelihood-based significance estimates in order to determine the 5σ discovery reach for the protophobic boson. We find that STCF can discover the protophobic boson while tolerating $\sim 10^4$ background events for specific regions of the parameter space around the 17 MeV peak. Our analysis establishes the first feasibility study of displaced light-boson searches at the STCF, motivating a full Geant-4 simulation.

Keywords: ATOMKI anomalies, Protophobic boson, Super tau-charm facility, TrackEff

1 Introduction

It might be tempting to think that the recent stress on the search for light new physics ($\lesssim 10$ GeV) is driven by the philosophy of searching under the lamppost. That it is being driven by the plethora of colliders running at \sim GeV energy scales, like the Belle II [1], BESIII [2], and GlueX [3]. However, on the contrary, the interest of the particle physics community has been piqued by such scenarios because of the substantial theoretical underpinnings on which they stand. Indeed, such sub-GeV particles are intimately linked with the Dark Matter (DM) content of the Universe, not only as the dark matter candidate [4–9], but also as portals between the visible- and the dark-sectors [10, 11]. In addition, light new physics (NP) is the natural corollary of one of the most elegant solutions to the strong CP problem [12–16]. Naturally, there is a concerted effort by the community to search for these [17–25].

In this paper, however, our focus is on one of the few remaining anomalies that challenges the particle content and interactions of the Standard Model (SM), giving rise to hopes of beyond the Standard Model (BSM) physics. There are intriguing observations pertaining to the transitions of light nuclei which are at tension with the SM of particle physics. These observations, corresponding to the E1, M0, and M1 nuclear transitions of elements like ${}^8\text{Be}$, ${}^{16}\text{O}$, ${}^4\text{He}$, ${}^{12}\text{C}$ have most recently been reported by the group at the ATOMKI facility in Debrecen, Hungary [26–31]. However, the anomalies persist from the middle of the 1990s [32–35]. These

*althaphysics@gmail.com

†gondogolegogol@gmail.com

different experiments report enhanced correlation between final state e^+e^- scattering angles, which cannot be explained by internal or external pair conversions. In response to these anomalies, the protophobic boson (X -boson), of mass $\simeq 17\text{ MeV}$, has been proposed as a promising NP model as a means to ameliorate the tensions [36, 37] (Also check, Refs. [38, 39] for comprehensive theoretical studies of the anomaly). In this work, we attempt to appraise the detection possibilities of the protophobic boson at the proposed Super τ -Charm facility (STCF) [40, 41].

The STCF is a proposed e^+e^- collider with a centre of mass (CoM) energy ranging from 3 GeV to 7 GeV , to be constructed in China, as an update to the BEPCII/BESIII experiment. The STCF is expected to produce a peak luminosity of $5 \times 10^{34} \text{ cm}^{-2}\text{s}^{-1}$ and an integrated luminosity of $15\text{ ab}^{-1} - 20\text{ ab}^{-1}$ per year), spread over staggered CoM energies [40, 41]. The interaction point (IP) is expected to be surrounded by a drift chamber—the main drift chamber (MDC)—in the barrel region. We propose to harness the tracking prowess of this MDC to look for displaced vertex (DV) signatures produced by the protophobic boson. We focus on the DV signatures as our interest lies in the intermediate coupling ranges, $\sim 10^{-3}$ to $\sim 10^{-6}$, a range over which the DV strategy works better than prompt or invisible searches [20, 21, 23].

In modelling the MDC, we use the framework `TrackEff`¹ [42] which has been published recently. `TrackEff` is essentially a `Python` module which allows us to model the detector geometry and the magnetic field for tracking detectors. The package takes in as input the location of the DV and the momenta of the final state charged tracks (e^-e^+ for our study). It then propagates the particle tracks in the magnetic field, computing the number of hits produced by them in the detector, using the detector geometry defined by us. In our simulations, we construct the STCF MDC geometry in `TrackEff` and define our criteria for a track to be ‘accepted’.

Our end goal is to compute the number of events per CoM energy per X -boson mass and coupling, given the known luminosity associated with each CoM energy. We focus on a small window around 17 MeV , where the X -boson is hypothesised to reside. For each parameter point, we compute the number of background events admissible for a 5σ significance discovery. We thus establish a baseline feasibility for the detection prospects of the X -boson at the STCF. Hence, we extend the physics goals of the STCF to solving one of the remaining unexplained phenomena left in particle physics.

It goes without saying that a full detector-level validation, using `Geant4` [43], is required to substantiate the claims about 5σ discovery. However, as mentioned above, our current aim is to establish a feasibility baseline using the `TrackEff` model. We note, in the lack of an actual detector, it is not possible to validate `TrackEff` against real STCF data. However, `TrackEff` has been cross-verified against real `Belle II` data and shows fidelity within 10% with data [42]. Given that, our results are expected to be conservative, at least at the order-of-magnitude level.

The paper is divided as follows, in [section 2](#) we list and describe the different anomalies recorded in the nuclear transitions by the ATOMKI group and by other collaborations, in [section 3](#) we discuss our parametrisation of the protophobic model, then in [section 4](#), we describe the STCF main drift chamber and how we model it in our code, in [section 5](#) we report our results, before concluding in [section 6](#).

2 The ATOMKI anomalies

Anomalous results in light nuclear transitions have persisted since the mid 1990s. We have given a snapshot of all these reports in [table 1](#). The first report was by the group at the Institut für Kernphysik, University of Frankfurt [32–34]. The group reported a deviation from expectations in the angular correlation of the final state electron-positron pairs [44–46] in the M1 e^+e^- decays of the 17.6 MeV level ($J^\pi = 1^+, T = 1$) of ${}^8\text{Be}$. Taking into account both internal pair conversion

¹<https://zenodo.org/records/1383199>, CC 4.0

(IPC) and external pair conversions (EPC) [47–49] does not explain the deviation. The same discrepancy was not observed in the E1 decays of the 17.2 MeV level ($J^\pi = 1^-, T = 1$) of ^{12}C . The deviation in the M1 decays had a significance of 4.5σ . The anomaly was observed for large values of the correlation angle ω . Both EPC and IPC fall off drastically for large separation angles [44], more so for low Z nuclei, hence, this anomaly was attributed to an exotic boson which was supposed to have been produced in the nuclear reaction. In the rest frame of the boson, the e^+e^- pair comes out back to back. In practice, the angle is smaller due to the Lorentz boost. A fit by the group predicted the mass of the exotic boson to be equal to 9 MeV.

Table 1: A list of all the anomalies reported in nuclear transitions which have been explained by an exotic boson of mass in the MeV ranges.

References	Transitioning Nucleus	Exotic Mass (MeV)
Ref. [32–34]	M1 decays of the 17.6 MeV and 14.6 MeV levels of ^8Be	9.0
Ref. [35]	M0 transition in the 10.95 MeV $0^- \rightarrow 0^+$ decay of ^{16}O	9.0 – 10.0
Ref. [26]	M1 decay of the 17.6 MeV level of ^8Be	12.0 ± 2.5
Ref. [27, 28]	M1 decays of the 17.6 MeV and 18.15 MeV levels of ^8Be	$16.70 \pm 0.35 \pm 0.50$
Ref. [29]	$^3\text{H}(p, \gamma)^4\text{He}$ reaction	$16.94 \pm 0.12 \pm 0.21$
Ref. [30]	E1 decay of the 17.2 MeV level of ^{12}C	$17.03 \pm 0.11 \pm 0.20$
Ref. [50]	M1 decay of the 17.6 MeV level of ^8Be	$16.66 \pm 0.47 \pm 0.35$
Ref. [31]	Giant Dipole Resonance decay of ^8Be	$16.95 \pm 0.48 \pm 0.35$

A similar deviation in the M1 decay of ^8Be was observed when the same experiment was repeated at the 1MV Van de Graaff accelerator of ATOMKI [26] in Debrecen, Hungary. The correlation in the angular separation was best explained by fitting e^+e^- pairs originating from the decay of a 12.0 ± 2.5 MeV exotic boson. The same group also reported a similar excess in the magnetic monopole, M0, transition of the 10.95 MeV $0^- \rightarrow 0^+$ transition of ^{16}O [35]. This discrepancy was explained by a boson of mass between 9.0 and 10.0 MeV.

A follow up experiment was performed at the 5MV Van de Graaff accelerator at ATOMKI [27, 28]. The first of these experiments focussed on the same M1 decay of ^8Be . This experiment did not find any substantial excess in the 17.6 MeV isovector transition but did find a discrepancy in the 18.5 MeV isoscalar transition at 6.8σ . The anomaly was explained by invoking an exotic boson with a fitted mass of $16.70 \pm 0.35 \pm 0.50$ MeV.

Not only the ^8Be system, such an anomaly was found in $^3\text{H}(p, \gamma)^4\text{He}$ reactions as well [29], in an experiment performed at the 2 MV Tandetron accelerator at ATOMKI. The peak in the angular correlation spectrum at a large angle, 115° , was explained by the creation and the subsequent decay of a light particle during the proton capture process to the ground state of the ^4He nucleus. The significance of the discrepancy varied between 6.6σ to 8.9σ for varying proton beam energies. The averaged value of the fitted mass of the exotic was found to be $16.94 \pm 0.12 \pm 0.21$ MeV.

Further support for the existence of the exotic boson came from the E1 decay of the 17.2 MeV level of ^{12}C . The correlation in the angular distribution, around 155 – 160° , was found in the E1 ground state decay of the 17.2 MeV $1^- \rightarrow 0^+$ transition of ^{12}C . This established the vectorial nature of the couplings of the exotic [37], the mass of which was fitted to be $17.03 \pm 0.11 \pm 0.20$ MeV. For different beam energies, the confidence for the fitted mass ranged from 3σ to 8σ .

The results at the ATOMKI accelerators were cross-checked at the 5SDH-2 Pelletron accelerator at the VNU University of Science at Hanoi, Vietnam [50]. The same ^8Be system was studied and the same excess in the angular separation of the e^+e^- was found at around 135° , at a significance greater than 4σ . The fitted mass of the exotic boson explaining the excess was found to be $16.66 \pm 0.47 \pm 0.35$ MeV.

To further test the vector nature of the exotic boson couplings, the decay of the giant dipole

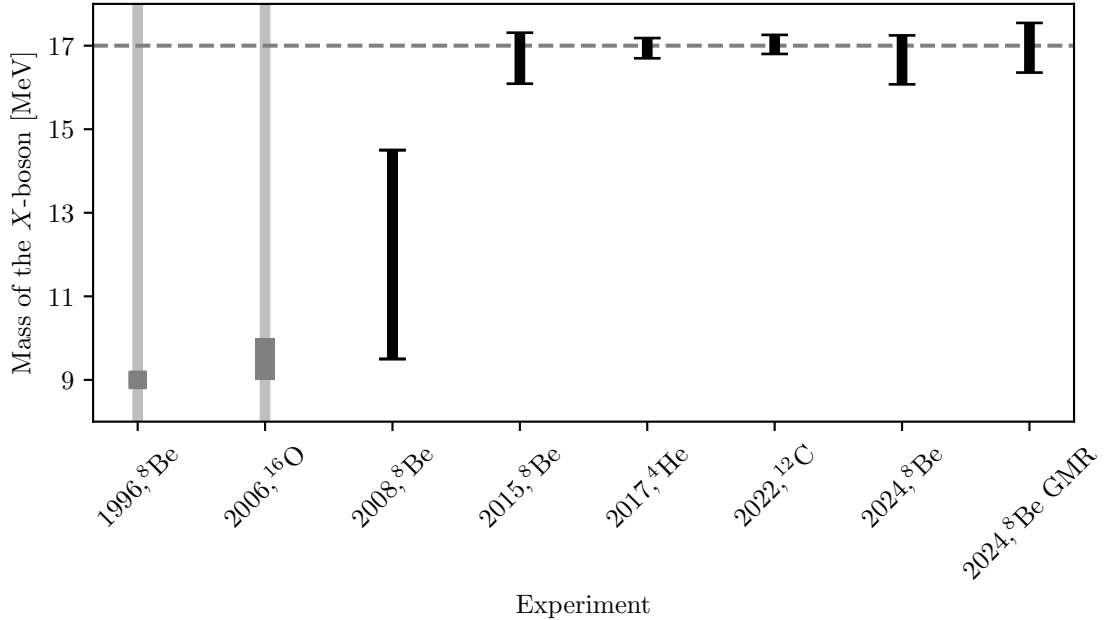


Figure 1: A compilation of the different results in support of the X -boson. The different experiments are indicated by the year of publication and the nucleus undergoing transition. Note, for the data points where error-bars are not given, we have taken the error to be larger than our scope of analysis. Details are given in the text.

resonance of ${}^8\text{Be}$ was studied, again at the 2 MV Tandetron accelerator of ATOMKI, Debrecen. The fit of the theoretical prediction of the E1+M1+exotic to the experimental data gives a $> 10\sigma$ confidence for the exotic. The measured invariant mass of the exotic was found to be $16.94 \pm 0.48 \pm 0.35$ MeV. For the different experiments, we have plotted the masses of the exotic bosons, predicted to solve the anomaly, in [fig. 1](#).

The results of all these experiments strongly indicate the presence of an exotic boson with vectorial couplings and a mass around 17 MeV. In this paper, we call this boson the X -boson, and the anomaly associated with it the ATOMKI anomalies. The anomalies have the following properties [\[50\]](#):

- The anomalies have been observed in the ${}^8\text{Be}$ system for different detector geometries.
- The anomalies have been observed using fundamentally different detector types: silicon strip detectors and multi-wire chambers
- The anomalies have been observed in four different nuclei, ${}^8\text{Be}$, ${}^4\text{He}$, ${}^{12}\text{C}$, and ${}^{16}\text{O}$.
- It shows up at varying e^+e^- opening angles consistent with the decay of a single particle
- The anomalies have been observed at different beam energies
- The anomalies have a very high statistical significance

A series of experiments, planned or running, have also been devised to establish the existence of the exotic boson. These include nuclear collision experiments at JINR, Dubna [\[51\]](#), at the Mu3e experiment [\[52\]](#), at the Montreal Tandem accelerator [\[53\]](#), at the JEDI experiment at GANIL, France [\[54\]](#), a new experimental setup at LNL, Legnaro [\[55\]](#), at the nTOF collaboration in CERN [\[56\]](#), and at the Pelletron accelerator in Melbourne [\[57\]](#). A detailed list of these experiments can be found in Ref. [\[58\]](#).

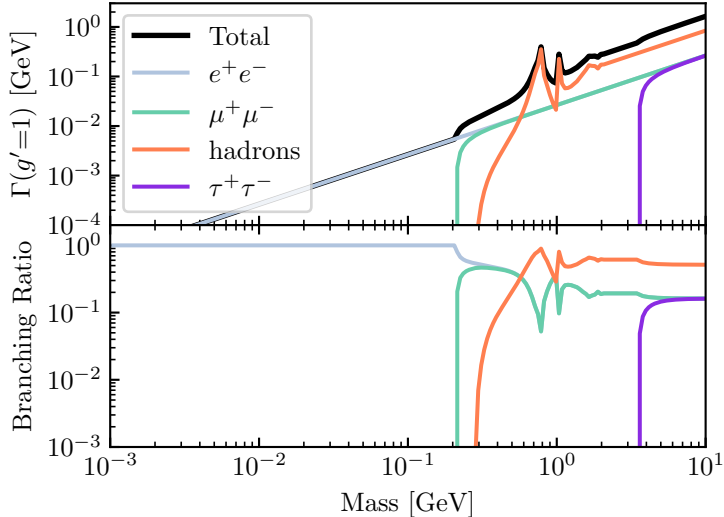


Figure 2: We plot the partial widths and the branching ratios of the X boson, for $\Gamma_{\text{DS}} = 0$. The top panel shows the partial widths and the bottom panel shows the branching ratios. The separate channels we consider are to taus, hadrons, muons, and electrons. We note, for $\Gamma_{\text{DS}} = 0$, the width is completely saturated by the electron channel below the muon mass.

It should be noted that the PADME experiments has recently published a result of collisions of positron beams on a fixed target. A dedicated search for the X -boson has led to the observation of a modest excess around 16.90 MeV with a significance of 2.5σ (local) and 1.8σ (global) [59]. On the other hand, no significant excesses were found in the same mass range in a search by the MEG II experiment [60].

The most obvious place to look for the origin of the piling up anomaly was in nuclear transition form-factors. However, the required form factor modifications were found to be unrealistic for ${}^8\text{Be}$ [61]. This has led to substantial efforts at model building leading to the invocation of both pseudoscalar and vector bosons [62–64] as the candidate X -boson. In this work, however, we focus on the protophobic boson hypothesis proposed to explain the anomaly [36]. We describe the necessary details of this model in the next section.

3 Model and Parametrisation

We consider the protophobic boson to be the gauge boson associated with the $U(1)_B$ of baryon number. Therefore, it couples to fermions with a charge equal to baryon number. The $U(1)_B$ symmetry is spontaneously broken to identity by a Higgs mechanism, generating mass for the X -boson. The $U(1)_B$ mixes kinematically with the $U(1)_{\text{EM}}$, with the Lagrangian:

$$\mathcal{L} \supset -\frac{1}{4}\tilde{F}^{\mu\nu}\tilde{F}_{\mu\nu} - \frac{1}{4}\tilde{X}^{\mu\nu}\tilde{X}_{\mu\nu} - \frac{\sin\chi}{2}\tilde{F}^{\mu\nu}\tilde{X}_{\mu\nu} + \frac{1}{2}(D_\mu\phi)^\dagger D^\mu\phi + \sum_f \bar{f}i\cancel{D}f. \quad (1)$$

Here, $\tilde{F}_{\mu\nu}$ and $\tilde{X}_{\mu\nu}$ are the field-strength tensors corresponding to the $U(1)_{\text{EM}}$ field and the $U(1)_B$ field respectively. The sum runs over all fermions f and we have

$$D_\mu\phi = \left(\partial_\mu + ie\epsilon_B B_\phi \tilde{X}_\mu\right)\phi, \quad (2)$$

$$D_\mu f = \left(\partial_\mu + ieQ_f \tilde{A}_\mu + ie\epsilon_B B_f \tilde{X}_\mu\right)f. \quad (3)$$

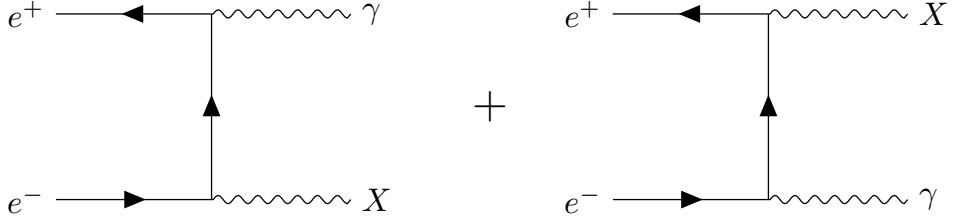


Figure 3: The t - and u -channel processes contributing to the production of the X -boson.

Here, \tilde{A}_μ and \tilde{X}_μ are the fields corresponding to the photon and the $U(1)_B$ respectively, Q_f and B_f are the electric charge and the baryon number of the fermion in question, and B_ϕ is the X -charge of the scalar. Finally, ee_B is the coupling strength associated with the X -boson.

To go to the canonically diagonal kinetic basis, we diagonalise the kinetic sector matrix via the triangular matrix

$$\begin{pmatrix} \tilde{A}^\mu \\ \tilde{X}^\mu \end{pmatrix} = \begin{pmatrix} 1 & -\tan \chi \\ 0 & \sec \chi \end{pmatrix} \begin{pmatrix} A^\mu \\ X^\mu \end{pmatrix}, \quad (4)$$

where A^μ and X^μ are the fields in the canonically diagonal basis. In this basis, the covariant derivatives become

$$D_\mu \phi = (\partial_\mu + ie\epsilon_B \sec \chi B_\phi X_\mu) \phi, \quad (5a)$$

$$D_\mu f = (\partial_\mu + ieQ_f A_\mu + ie(-Q_f \tan \chi + \epsilon_B B_f \sec \chi) X_\mu) f. \quad (5b)$$

Now, imposing, $\epsilon_B \equiv \sin \chi$, we get the charges of the fermions, as given in table 2. The

Table 2: The charges of the fermions of one generation in units of $e \tan \chi$.

Fermion	q_u	q_d	e	ν
Charges	$-\frac{1}{3}$	$\frac{2}{3}$	1	0

corresponding covariant derivatives are:

$$D_\mu \phi = (\partial_\mu + ie \tan \chi B_\phi X_\mu) \phi, \quad (6a)$$

$$D_\mu f = (\partial_\mu + ieQ_f A_\mu + ie \tan \chi X_f X_\mu) f. \quad (6b)$$

Then $g' = e \tan \chi$ is the effective coupling strength of the X -boson, and $X_f = B_f - Q_f$ is the effective charge of the fermion f . Now, once the scalar ϕ acquires a vev $\phi \rightarrow \phi + v_\phi$, the gauge boson X_μ acquires a mass, $m_\chi^2 = e^2 \tan^2 \chi B_\phi^2 v_\phi^2$. For the couplings we are looking at, $g' \sim 10^{-3} - 10^{-6}$ GeV, the singlet scalar ends up in the multi TeV ranges, and is safe from constraints. Note that, we are writing the charges much below the electroweak symmetry breaking scale. Also, $\epsilon_B = \sin \chi$ can only be imposed at any one scale in the evolution of the coupling. The two entities will renormalise differently as the scale runs. However, we can always set the equality at ~ 17 MeV so that we don't have to worry about running effect in the narrow window around ~ 17 MeV, where we concentrate.

Also note, the $U(1)_B$ symmetry is anomalous as the gauge currents do not cancel either mixed-gauge or gauge-gravity anomalies with the SM particle content. However, this has to be viewed in context. As we are performing a low-energy study, our theory can always be viewed as the remnant of a UV-complete theory where anomaly cancellation is ensured by additional chiral (under $U(1)_B$) fermions above the electroweak scale (check, e.g., Ref. [36]).

In order to expand the scope of the model, we allow the X -boson to couple to a generic dark sector as well. We remain agnostic about the details of the dark sector and do not speculate on

the nature of the couplings, nor do we fix the possible particle content. Instead, we consider the partial decay width to the dark sector, which we use as a parameter of the model:

$$\begin{aligned}\Gamma_{\text{Tot}} &= \Gamma_{\text{VS}} + \Gamma_{\text{DS}}, \\ \text{with, } \Gamma_{\text{VS}} &= \Gamma_e + \Gamma_\mu + \Gamma_h + \Gamma_\nu + \Gamma_\tau,\end{aligned}\tag{7}$$

where, Γ_{Tot} indicates the total decay width. Γ_{VS} and Γ_{DS} indicate the partial widths to the visible and the dark sectors. The visible sector width is further broken into Γ_e , Γ_μ , Γ_ν , Γ_h , Γ_τ , which are the partial widths to electrons, muons, hadrons, neutrinos, and taus respectively. For this analysis, we will work with three benchmark points [65]:

$$\Gamma_{\text{DS}} = 0; \quad \Gamma_{\text{DS}} = 10\Gamma_{\text{VS}}; \quad \Gamma_{\text{DS}} = \Gamma_{\text{VS}}/10.\tag{8}$$

The partial widths are straightforward to compute both above Λ_{QCD} and below the pion mass, for which

$$\Gamma_{X \rightarrow f\bar{f}} = \frac{n_c^f}{3} \alpha_{\text{EM}} g'^2 X_f^2 m_X \sqrt{1 - 4 \frac{m_f^2}{m_\chi^2}} \left(1 + 2 \frac{m_f^2}{m_X^2}\right),\tag{9}$$

where, $n_c^f = 1, 3$ for leptons and quarks respectively. However, for $m_X \sim \Lambda_{\text{QCD}}$, we have to compute the decay widths to final state hadrons, using an appropriate effective Lagrangian. A variety of approximate techniques are used to compute the decay widths in this region. We implement the data-driven approach within the vector meson dominance framework, as given in Ref. [18], to get the widths. Specifically, we use the companion package of Ref. [18], `DarkCast`² to obtain the decay widths. We have shown the partial widths and the branching fractions of the X -boson in fig. 2 for $\Gamma_{\text{DS}} = 0$.

The quark-level effective Lagrangian we work with is

$$\mathcal{L} \supset -\frac{1}{4} X_{\mu\nu} X^{\mu\nu} + \frac{1}{2} m_X^2 X_\mu X^\mu + ig' \sum_f X_f \bar{f} \not{X} f + X_\mu \sum_i O_i^\mu + F_{\mu\nu} \sum_i O_i^{\mu\nu}.\tag{10}$$

where f are the SM fermions, X_f is the X -boson charge of f , and O_i^μ and $O_i^{\mu\nu}$ are dimension three and higher dimensional dark sector operators interacting with the X_μ gauge field and the field-strength tensor, respectively.

We rely on the t - and u -channel production of the X -boson in association with a photon, as given in fig. 3. The production of the X -boson is independent of the properties of the dark sector. It depends only on the coupling of the X -boson to the electron. The cross-section of production for $e^+e^- \rightarrow X\gamma$ is given by:

$$\frac{d\sigma}{d\eta} = \frac{\alpha_{\text{EM}}}{2s} (g' X_f)^2 \frac{\cos^2 \vartheta(\eta) (s - m_\chi^2)^2 + (s + m_\chi^2)^2}{s(s - m_\chi^2)},\tag{11}$$

where $\vartheta(\eta) = 2 \arctan(e^{-\eta})$. Naturally, there is a t -channel enhancement towards large angles, as can be seen in the differential cross-section plot in the left panel of fig. 4, where the solid orange line represents our analytical calculations. The total cross section is not sensitive to the mass of the X -boson as the boson mass is much less than the CoM energy. However, the cross-section varies with the CoM energy, as given in the right panel of fig. 4.

Having discussed the production and the decay mechanisms of the X -boson, in the next section we discuss the details of the STCF, especially its drift chamber in order to explain how we intend to observe the displaced vertices produced by it.

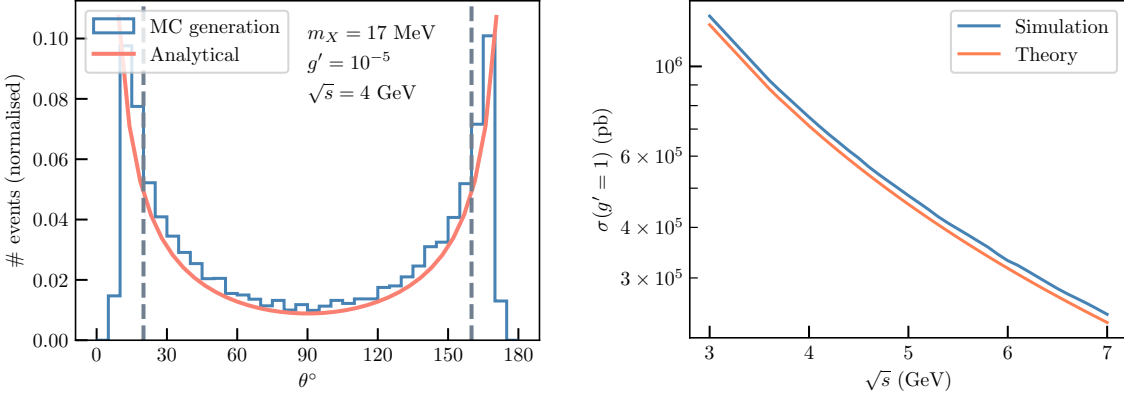


Figure 4: Left: We plot the differential cross section as a function of the scattering angle, θ for $m_X = 17 \text{ MeV}$, $g' = 10^{-5}$, $\sqrt{s} = 4 \text{ GeV}$. We plot the cross sections generated from MC simulations in MG5_aMC, and calculated from eq. (11). We have indicated the lower and upper angular cuts of $\theta = 20^\circ$ and $\theta = 160^\circ$ that we impose at analysis level. Right: We plot the total cross section as a function of CoM energies.

Table 3: CoM energies and corresponding integrated luminosities projected for STCF Phase-I [40]. The 4–7 bucket indicates a 300-point scan with 10 MeV steps, with 10 fb^{-1} per point.

\sqrt{s} (GeV)	3.097	3.67	3.686	3.770	4.009	4.180	4.230	4.360	4.420	4.630	4.0 – 7.0
\mathcal{L}_{int} (ab $^{-1}$)	1	1	1	1	1	1	1	1	1	1	3

4 The STCF main drift chamber

The STCF is a proposed e^-e^+ collider with symmetric beam energies and CoM energies between 2 GeV to 7 GeV. The peak instantaneous luminosity is $0.5 \times 10^{35} \text{ cm}^{-2}\text{s}^{-1}$ corresponding to a CoM energy of 4 GeV in Phase I. It is on phase I that we exclusively concentrate in this work. The integrated luminosities corresponding to the different CoM energies are given in table 3 [41]. STCF projects to have hardware and software upgrades leading to lower backgrounds than current flavor experiments like Belle-II and LHCb, almost 100% detection efficiencies, and almost full detector acceptance [40]. Although, these estimates are aspirational, they help us in modeling this initial study.

In the barrel region, the STCF detector complex consists of an inner silicon tracker, surrounded by the MDC, surrounded by a RICH detector for particle identification, which is enclosed inside the electromagnetic calorimeter, surrounded by a superconducting magnet producing 1 T magnetic field, with a polar coverage of 93%. The outermost layer is a muon counter. Out of these, only the MDC is of importance to us in this paper.

In fig. 5 we have drawn cartoons of the cross-section and the longitudinal-section of the STCF MDC, as obtained from their Technical Design Report (TDR) on detectors [40]. The MDC extends in the radial direction from 20 cm to 83 cm, with a total of 48 layers of drift cells. The drift cells are arranged in 8 superlayers, the details of which are given in table 4. The cell dimensions are designed to range from 0.98 – 1.25 cm in the innermost superlayer to 1.33 – 1.45 cm in the outermost superlayer.

The MDC is expected to i) measure momentum with an excellent resolution of $< 0.5\%$ at 1 GeV, ii) reconstruct charged tracks in tandem with the inner trackers, and iii) measure the energy loss of the particles (dE/dx) for PID. The track reconstruction methods and algorithms

²<https://gitlab.com/philten/darkcast>, GNU GPL V2

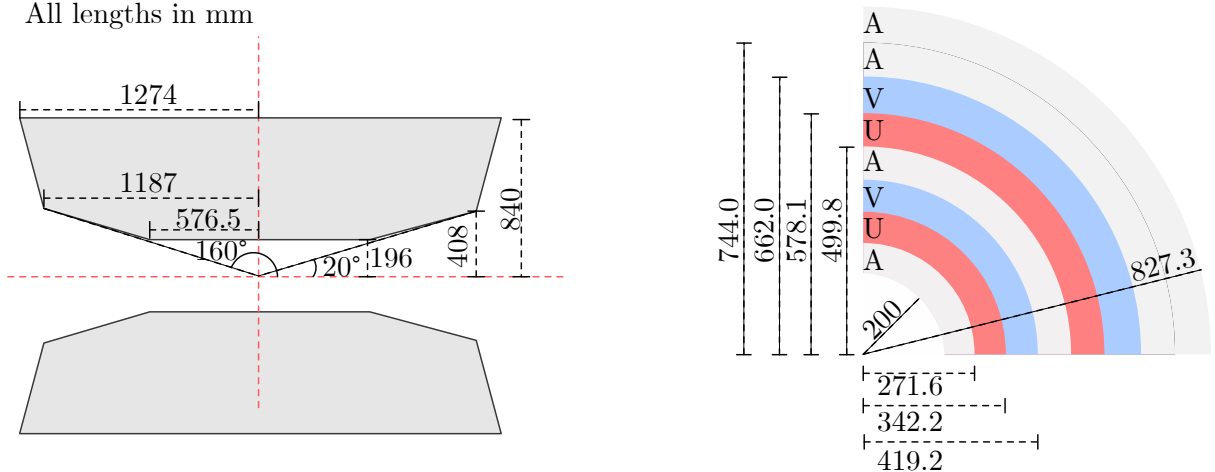


Figure 5: Cross-sectional (right) and longitudinal (left) views of the STCF main drift chamber. We show the relevant lengths in both the views (all lengths in mm). In the cross-sectional view we show the different superlayers in the MDC with both axial (A) and stereo (U,V) arrangements.

Table 4: Details of the STCF main drift chamber components [40]. ‘A’ represents an axial layer while ‘U’ and ‘V’ represent stereo layers.

Superlayer	Radius (mm)	# layers	Stereo Angle (mrad)	# cells	Cell Size (mm)
A	200.0	6	0	128	9.8 – 12.5
U	271.6	6	39.3 – 47.6	160	10.7 – 12.9
V	342.2	6	-41.2 – -48.4	192	11.2 – 13.2
A	419.2	6	0	224	11.7 – 13.5
U	499.8	6	50.0 – 56.4	256	12.3 – 13.8
V	578.1	6	-51.3 – -57.2	288	12.6 – 14.0
A	662.0	6	0	320	13.0 – 14.3
A	744.0	6	0	352	13.3 – 14.5
Total	200 – 827.3	48		11520	

planned for STCF have been rigorously studied in Refs. [66, 67]. In this work we rely on the tracking efficiency of the MDC exclusively, and do not take into account the inner trackers as the inner trackers are too close to the IP for SM displaced vertex processes to dominate. We model the STCF MDC detector geometry using the `TrackEff` package [42], and it is with the help of `TrackEff` that we obtain the vertex reconstruction efficiency (VRE). The 48 layers of the MDC are grouped into superlayers, each containing 6 layers. The number of drift cells in the $r\text{-}\phi$ plane increases from 128 in the innermost layer to 352 in the outermost layer. The drift cells are approximately squares in cross-section, with the size gradually increasing within each superlayer. This morphology was implemented in `TrackEff`.

Using the momentum and the position of the decay vertex of the X -boson, obtained from our simulations, `TrackEff` reconstructs the trajectories of the daughter electrons by propagating them through the uniform magnetic field, of 1 T, inside the fiducial volume of the detector. The path of each trajectory in each drift cell is divided into n_s segments of length Δ_s . In our analysis we assume the default length size of $\Delta_s = 1$ mm. The minimum n_s required within a drift cell of each layer can be adjusted to control the hit acceptance criteria. To account for the increasing cell size within each superlayer, we modified the `TrackEff` configuration to reflect the MDC layer arrangement. We set this threshold to $n_s^{\text{inner}} = 5$ for cells in the innermost superlayer, while for the remaining superlayers we use $n_s = 10$. This choice ensures that smaller cells near the

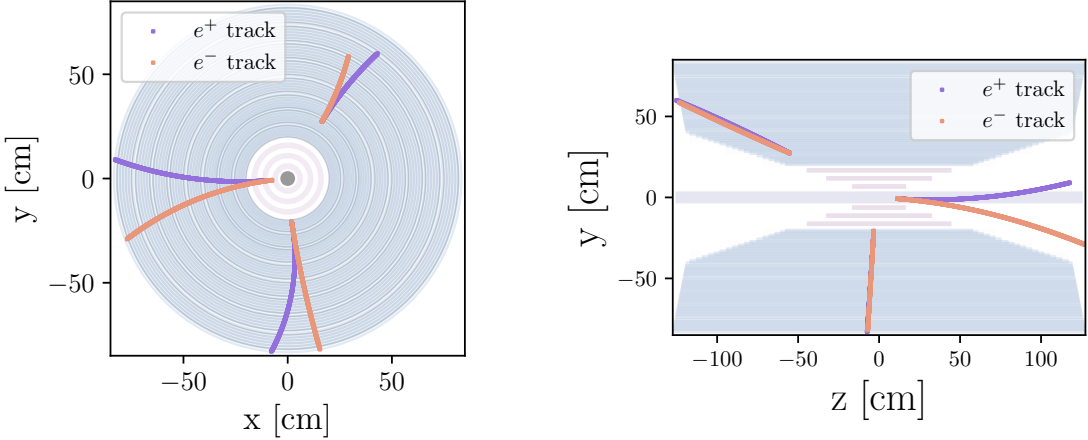


Figure 6: Cross-sectional (left) and Longitudinal sectional (right) view of the modelled STCF MDC inside `TrackEff`. We also show three typical events in both the views. The red lines are the electron tracks while the blue lines are the positron tracks.

interaction point, more sensitive to highly boosted tracks, require fewer steps, whereas the larger cells at higher radii require more steps to maintain consistent hit acceptance. For a track to be considered reconstructed, we require it to have produced hits in at least 24 detector cells.

In fig. 6 we plot the `TrackEff` representation of the MDC. We plot both the cross-section and the longitudinal-section. For reference, we have shown the beam-pipe and the inner trackers. We show three pairs of tracks from our simulations arising at different distances from the IP. The red and the blue lines represent electron and positron tracks respectively. Having discussed all the required pieces that goes into our actual analysis, in the next section we give the actual analysis details and our findings.

5 Analyses and Results

For our analyses we generated 10^4 events per mass point per CoM energy in `MG5_aMC@NLO`³ [68]. Instead of a 300-point scan of the $4 - 7$ GeV range with 10 fb^{-1} per point (table 3), we perform a 30-point scan with 100 fb^{-1} per point. The total number of events we work with per mass-coupling point is then 4×10^5 , corresponding to the CoM energies given in table 3. The cross-sections obtained from the event generator is in close agreement to the analytically computed cross-section as given in eq. (11). We plot the total and differential cross-section as obtained from `MG5_aMC@NLO` in fig. 4, for $m_X = 17 \text{ MeV}$ and $\sqrt{s} = 4 \text{ GeV}$. We overlay the analytically computed differential cross-section for the same m_X and \sqrt{s} . The total cross-section varies only slightly with the mass of the X -boson and is approximately equal to $7 \times 10^6 \text{ pb}$ over the mass range of interest, for $g' = 1$. The variation with the CoM energy is more pronounced, and is depicted in fig. 4. The expected number of DV events per CoM energy, as computed from the cross-section is then:

$$N^i(m_X, g', \Gamma_{DS}) = \mathcal{L}_{\text{int}}^i \times \sigma^i(m_X, g') \times \text{BR}(m_X, \Gamma_{DS}) \times \text{eff}^i(m_X, g', \Gamma_{DS});$$

with, $N_{\text{tot}} = \sum_i N^i$. (12)

The superscript i indicates that the number of events are separately computed for the different \sqrt{s} points given in table 3, before combining. Here, N^i is the number of events, $\mathcal{L}_{\text{int}}^i$ is the

³<https://launchpad.net/mg5amcnlo>, Open Source

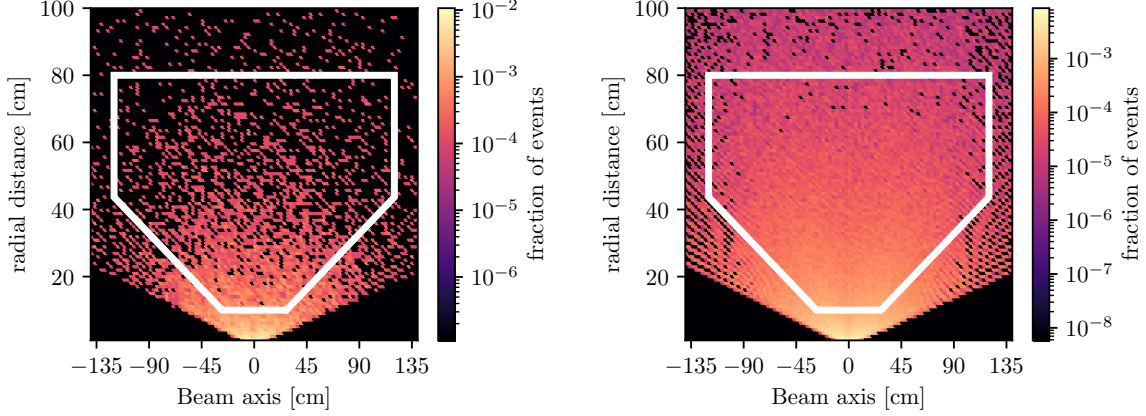


Figure 7: Heatmaps showing the distribution of the decay vertex of the X -boson. We have plotted the outline of the region of acceptance of vertices in white. The left panel shows the plot for events at $\sqrt{s} = 4$ GeV and the right panel is for events for all the luminosities added together. The parameter point considered is $m_X = 17$ MeV and $g' \sim 10^{-5}$, which translates to $\beta\gamma c\tau \simeq 49$ cm.

integrated-luminosity, σ^i is the cross-section of $e^+e^- \rightarrow \gamma X$, BR is the branching ratio of the X -boson to two electrons, and eff^i is the overall detection efficiency of the displaced vertex. We have explicitly shown the dependence of the objects on the three parameters of our model, m_X , g' , and Γ_{DS} . The total number of events, over all CoM energies, is $N_{\text{tot}} = \sum_i N_i$.

The generated events are binned by scattering angle, in bins of 1° . The X -bosons produced in each bin are made to decay at a random distance away from the IP, as per the exponentially falling decay distribution:

$$P(l) = \frac{1}{\lambda} e^{-\frac{l}{\lambda}}, \quad (13)$$

where, $P(l)$ is the probability of decaying at a distance l from the IP and λ is the characteristic decay length of the hypothetical boson, defined by

$$\lambda = \beta\gamma c\tau \quad (14)$$

where $\beta\gamma = |\vec{p}|/m_X$ is the Lorentz boost factor of the produced X -boson, c is the velocity of light in vacuum, and $\tau = 1/\Gamma_{\text{Tot}}$ is the characteristic decay time of the X -boson, with Γ_{Tot} being its total decay width. The branching fractions and the decay widths are both obtained using the methods discussed in [section 3](#).

Table 5: Listed are the cuts that we impose on our events. The p_T^ℓ cut is on the electrons and positrons which are produced from the X -boson decay. The geometric cuts are all on the position of the displaced vertex.

p_T^ℓ	l_{\min}	l_{\max}	z_{\min}	z_{\max}	θ_{\min}	θ_{\max}
0.1 GeV	10 cm	80 cm	-120 cm	120 cm	20°	160°

We apply a series of analysis-level cuts on the position of the decay vertices of the produced X -boson and on the momenta of the produced e^+ and e^- . These cuts have been noted in [table 5](#). The cut on the momenta of the daughter e^+ and e^- has been imposed for efficient track reconstruction. In [appendix A](#), we demonstrate the effect of varying this cut on discovery potential. The lower limit on the distance, l_{\min} , ensures that we are far away from the IP for

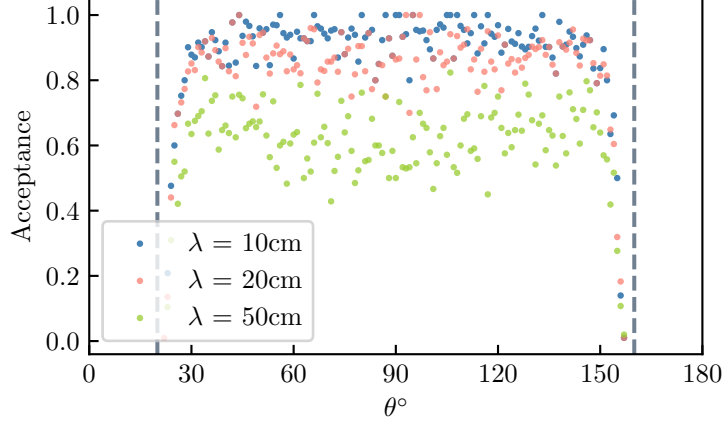


Figure 8: We plot the vertex reconstruction efficiency distribution as a function of the scattering angle, binned in 1° bins. We find that the efficiency drops drastically for large angles, near our angular cuts.

long-lived SM backgrounds from $K_S^0 \rightarrow \pi^+\pi^-$, $\Lambda \rightarrow p\pi^-$ to drop off [20, 23]. The upper limit, l_{\max} , is determined by the extent of the detector. As we pass the events through another layer of selection through `TrackEff`, which checks if the event translates to reconstructible tracks, we keep the upper limit aggressively close to the detector endpoint at this level.

In [fig. 7](#) we plot a particular instance of our simulation. We show the spatial location of the decay vertices of the X -boson for the 10^4 events we generate for $m_X \sim 17$ MeV and $g' = 10^{-5}$. This translates to $\beta\gamma c\tau \simeq 49$ cm⁴. To increase readability, we have plotted the fraction of events per bin. We have binned the vertices on a 100×100 grid, from -140 cm to 140 cm in the z direction and from 0 cm to 100 cm in the radial direction. In the left panel we have plotted the 10^4 simulated event corresponding to $\sqrt{s} = 4$ GeV and in the right panel we have plotted all the 4×10^5 events combining the different CoM energies given in [table 3](#).

It is clear that most of the X -bosons still decay near the IP, despite a large characteristic decay length. This is by virtue of the exponential decay distribution the events follow. However, we find that owing to the large number of events, there are decay vertices distributed throughout the MDC. Note, at generation level we have imposed a cut on rapidity of $|\eta| = 2.5$ ($\theta \sim 10^\circ$), hence, there are no events in the corresponding region in [fig. 7](#).

The e^+e^- tracks produced at the site of the X -boson decay vertex are passed through `TrackEff` to see which tracks are accepted as per the selection criteria discussed in the last section. After performing the analysis over 4×10^5 events for each parameter point, we multiply the number of accepted events by the relevant efficiency factor. Note, the number of accepted events indicate the number of events reconstructed after passing through our simulation chain. An event is considered accepted when both the tracks corresponding to the event are reconstructed. The acceptance constitutes the detector efficiency in [eq. \(12\)](#). It is defined as:

$$\text{eff}^i = \frac{N_{\text{acc}}^i}{N_{\text{MC}}^i}, \quad (15)$$

where N_{MC} is the total number of MC generated events which pass the cuts given in [table 5](#), and N_{acc} are the events out of it which are reconstructed by `TrackEff`. The i superscript again indicates the CoM energy.

In [fig. 8](#) we plot eff^i for a certain set of events. We generate 10^4 events corresponding to $\beta\gamma c\tau = 10$ cm, 20 cm, and 49 cm. We then bin the events in 1° bins. For all the generations, we

⁴As for two body decay $|\vec{p}| = \frac{s-m^2}{2\sqrt{s}}$.

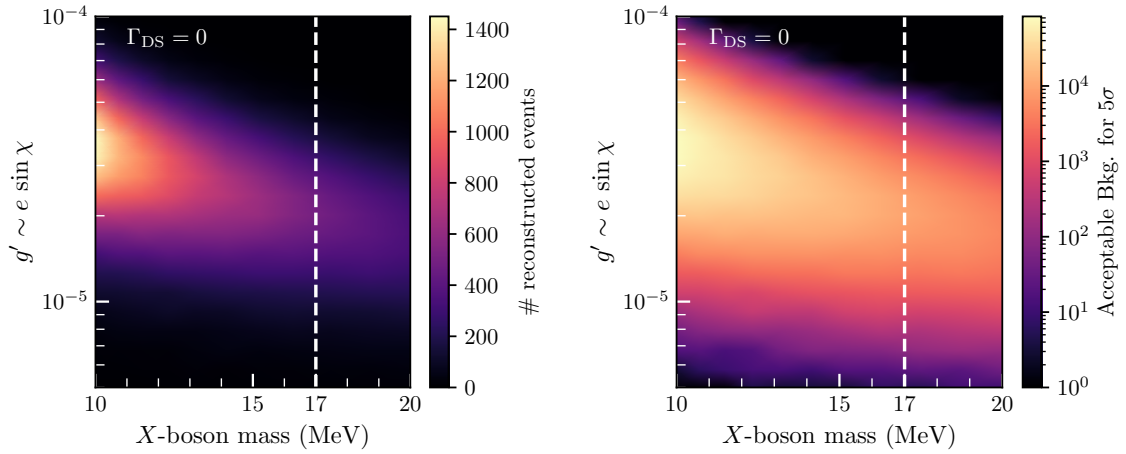


Figure 9: On the left panel we plot the number of signal events after detector simulation via `TrackEff`, as a function of the mass of the X -boson and its coupling strength. The corresponding colormap uses a linear scale. On the right panel, we plot the number of background events that can be tolerated for 5σ discovery of the X -boson, as a function of the same mass and couplings. The corresponding colormap is in log scale. As per the requirements of the ATOMKI anomaly, we have concentrated on a small window of masses around 17 MeV.

have $m_X = 17$ MeV. The point corresponding to a bin represents the ratio of the number of events accepted (by `TrackEff`) to the number of events generated. We note, as the decay length increases, the plot becomes more erratic. This is expected as the number of detector layers available to a track generated far away from the IP will be much less. Hence, the transversality of the track will play an important role. Tracks which are more longitudinal will have access to more cells to hit than tracks which are more transverse. Also, note that the acceptance falls drastically at large and small angles. This is due to the detector geometry, as discussed in the last section. In fact, the falling off happens exactly at the geometric cuts that we have imposed at $\theta = 20^\circ$ and 160° .

Although we consider displaced vertices far away, 10 cm, from the IP to mitigate SM background, we do not get a background-free environment. There will still be SM displaced tracks predominantly due to $K_S^0 \rightarrow \pi^+ \pi^-$ and $\Lambda \rightarrow p \pi^-$ [69] decays. Also, there will be backgrounds from pair production by photons interacting with the detector material [21, 24]. In addition, hadronic interactions with the detector material will produce mesons, protons, and nuclear fragments which will give rise to tracks. There will also be backgrounds from coincidental crossing of tracks [69]. It is beyond the scope of this paper to perform the necessary detector simulations to estimate the exact fraction of background events that survive the cuts, as backgrounds for displaced vertices necessarily requires a simulation of interaction of radiation with matter. To compensate for this, we keep the number of background events as a parameter of our search. Instead of presenting a deterministic 5σ contour of discovery, we find out the number of background events which can be tolerated for 5σ discovery, per mass and coupling point.

The median discovery significance, with s number of signal events and b number of background events is given by [70–73]:

$$Z_{\text{disc}} = \sqrt{2[(s+b) \ln(1+s/b) - s]} . \quad (16)$$

We solve eq. (16) as a function of b with $Z_{\text{disc}} = 5$, to find the number of background events admissible. The signal events, s , are what we find in our simulations, *i.e.*, as given in eq. (12).

In the left panel of fig. 9, we plot the number of true events corresponding to the mass and the coupling of the X -boson, as obtained from eq. (12) and eq. (15). In the right panel

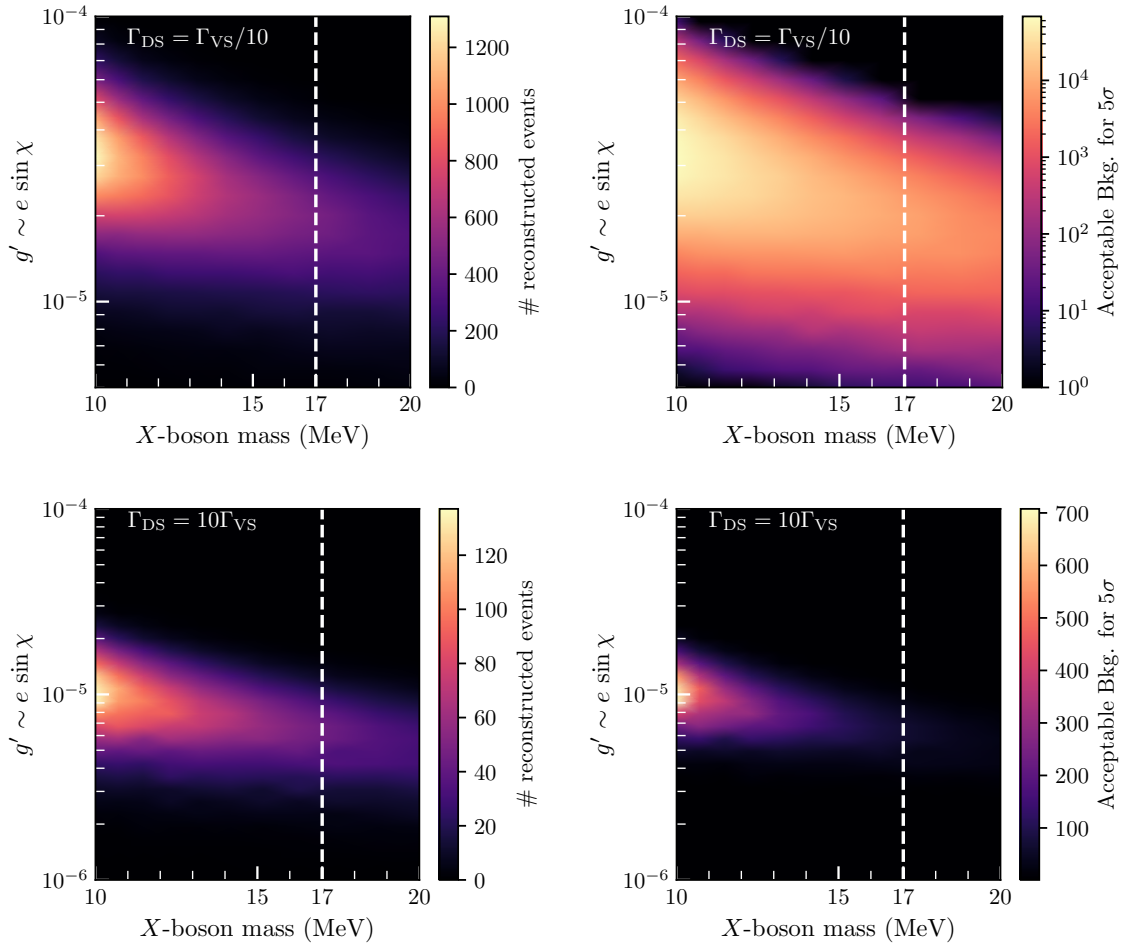


Figure 10: On the left panel we plot the number of signal events after detector simulation via `TrackEff`, as a function of the mass of the X -boson and its coupling strength. The corresponding colormap uses a linear scale. On the right panel, we plot the number of background events that can be tolerated for 5σ discovery of the X -boson, as a function of the same mass and couplings. The corresponding colormap is in log scale. As per the requirements of the ATOMKI anomaly, we have concentrated on a small window of mass around 17 MeV.

of fig. 9, we plot the number of background events that can be tolerated to produce 5σ discovery significance, as dictated by eq. (16). From fig. 9, it is clear that for extended regions of the parameter space around 17 MeV, the X -boson search can tolerate up to 10^4 background events for 5σ discovery. Note the different scaling of the colourmaps in the two figures. The left panel uses a linear scaling while the right panel uses a logarithmic scaling.

We repeat the same exercise for the two other branchings given in eq. (8). For $\Gamma_{DS} = \Gamma_{VS}/10$, we do not expect much difference from the $\Gamma_{DS} = 0$ case. This is exactly what the plots in the top two panels of fig. 10 show. However, for $\Gamma_{DS} = 10\Gamma_{VS}$, the situation is dramatically different, as for discovery, the number of backgrounds need to be extremely low—a few hundreds of events. Therefore, if the X -boson predominantly couples to a dark sector, the chances for detection, via displaced vertex searches will go down drastically. Other search techniques, like invisible searches need to be used in that case.

6 Conclusion

The anomalies in nuclear transitions reported by the ATOMKI collaboration provide us with overwhelming hints of physics beyond the Standard Model. The protophobic model is a prime candidate that ameliorates the tension between theory expectations and experimental observations. However, some negative results, like the one reported by MEG-II [60], and tensions with electroweak precision observables [74] implore us to keep looking for the protophobic boson at other experimental facilities. In this work, we initiate this effort for the proposed Super τ -Charm Facility (STCF). We observe that a protophobic boson of mass around 17 MeV can be discovered at 5σ C.L. by the STCF for background events as large as 10^4 . In essence, this work gives another use case to the already rich STCF physics programme. Our results are hopeful enough for the members of the STCF collaboration to cross-check them using vetted fast simulators and more efficient detector simulation using dedicated programs like GEANT-4.

Acknowledgements: We thank Jim Libby, Biplob Bhattacherjee, Anindya Datta, and Gautam Bhattacharyya for useful discussions and suggestions. Other than the packages mentioned in the text, all computations and visualisations have been done using Python 3.13.7 and its scientific stack of Numpy [75], SciPy [76], and Matplotlib [77].

A Results for varying p_T cuts

The analyses in our main text is crucially based on the STCF claim of targeting near 100% detection efficiencies [40, 67, 78] of charged tracks above $p_T^\ell = 0.3$ GeV and about 90% efficiency for lower than that, till 0.1 GeV. As a result, we imposed a mild p_T^ℓ cut on the charged tracks of 0.1 GeV. In this appendix we explore the effects of imposing stronger p_T^ℓ cuts on the final state leptons. This is a contingency study in case STCF fails to reach its aspirational numbers.

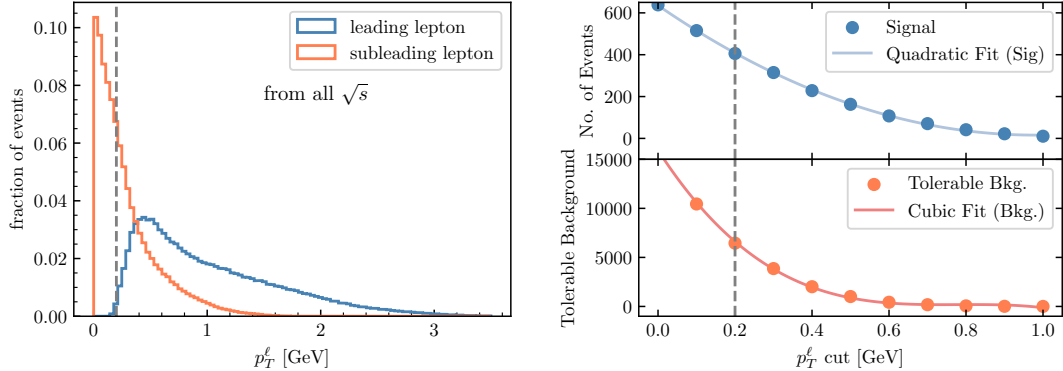


Figure 11: In the left panel we bin the leading and subleading leptons according to their transverse momentum. In red we show the number of subleading leptons per transverse momentum bin and in blue we show the number of leading leptons per bin. In the right panel we plot the number of accepted signal events for different p_T^ℓ cuts (blue). With an increasing cut value, the number of signal events drop off quadratically. We also plot the corresponding tolerable background (red) for 5σ discovery. We find that it drops off as a cubic.

In the left panel of fig. 11, we plot the p_T of the leading and subleading leptons for all the events we generated across the different \sqrt{s} . The figure makes it clear that a large fraction of subleading leptons have p_T less than 0.2 GeV. Here, we focus on 0.2 GeV as BESIII can efficiently track charged particles till that threshold [79–81].

In the right panel of the figure, we choose a mass-coupling point, $17.5 \text{ MeV} - 2 \times 10^{-5}$, and compute the number of accepted events for different p_T^ℓ cuts ranging from $p_T^\ell = 0$ GeV to

$p_T^\ell = 1$ GeV. We find that the number of signal events fall off quadratically with an increasing p_T^ℓ cut. We also plot the corresponding background events that can be tolerated for 5σ discovery and find that it falls as a cubic with an increasing p_T^ℓ cut. What the figure tells us is that for a p_T^ℓ cut between 0.1 GeV and 0.2 GeV, we can tolerate between ~ 9000 to ~ 5000 background events for a 5σ discovery. For calculating the number of signal events, we have used $\Gamma_{\text{DS}} = 0$.

References

- [1] T. Abe et al. “Belle II Technical Design Report”. In: (Nov. 2010). arXiv: 1011.0352 [physics.ins-det].
- [2] D. M. Asner et al. “Physics at BES-III”. In: *Int. J. Mod. Phys. A* 24 (2009), S1–794. arXiv: 0809.1869 [hep-ex].
- [3] S. Adhikari et al. “The GLUEX beamline and detector”. In: *Nucl. Instrum. Meth. A* 987 (2021), p. 164807. DOI: 10.1016/j.nima.2020.164807. arXiv: 2005.14272 [physics.ins-det].
- [4] John Preskill, Mark B. Wise, and Frank Wilczek. “Cosmology of the Invisible Axion”. In: *Phys. Lett. B* 120 (1983). Ed. by M. A. Srednicki, pp. 127–132. DOI: 10.1016/0370-2693(83)90637-8.
- [5] L. F. Abbott and P. Sikivie. “A Cosmological Bound on the Invisible Axion”. In: *Phys. Lett. B* 120 (1983). Ed. by M. A. Srednicki, pp. 133–136. DOI: 10.1016/0370-2693(83)90638-X.
- [6] Michael Dine and Willy Fischler. “The Not So Harmless Axion”. In: *Phys. Lett. B* 120 (1983). Ed. by M. A. Srednicki, pp. 137–141. DOI: 10.1016/0370-2693(83)90639-1.
- [7] Gianfranco Bertone, Dan Hooper, and Joseph Silk. “Particle dark matter: Evidence, candidates and constraints”. In: *Phys. Rept.* 405 (2005), pp. 279–390. DOI: 10.1016/j.physrep.2004.08.031. arXiv: hep-ph/0404175.
- [8] Jonathan L. Feng. “Dark Matter Candidates from Particle Physics and Methods of Detection”. In: *Ann. Rev. Astron. Astrophys.* 48 (2010), pp. 495–545. DOI: 10.1146/annurev-astro-082708-101659. arXiv: 1003.0904 [astro-ph.CO].
- [9] Karim Ghorbani. “Light vector dark matter with scalar mediator and muon g-2 anomaly”. In: *Phys. Rev. D* 104.11 (2021), p. 115008. DOI: 10.1103/PhysRevD.104.115008. arXiv: 2104.13810 [hep-ph].
- [10] C. Boehm and Pierre Fayet. “Scalar dark matter candidates”. In: *Nucl. Phys. B* 683 (2004), pp. 219–263. DOI: 10.1016/j.nuclphysb.2004.01.015. arXiv: hep-ph/0305261.
- [11] Pierre Fayet. “Light spin 1/2 or spin 0 dark matter particles”. In: *Phys. Rev. D* 70 (2004), p. 023514. DOI: 10.1103/PhysRevD.70.023514. arXiv: hep-ph/0403226.
- [12] Gerard ’t Hooft. “Symmetry Breaking Through Bell-Jackiw Anomalies”. In: *Phys. Rev. Lett.* 37 (1976). Ed. by Mikhail A. Shifman, pp. 8–11. DOI: 10.1103/PhysRevLett.37.8.
- [13] R. D. Peccei and Helen R. Quinn. “CP Conservation in the Presence of Instantons”. In: *Phys. Rev. Lett.* 38 (1977), pp. 1440–1443. DOI: 10.1103/PhysRevLett.38.1440.
- [14] R. D. Peccei and Helen R. Quinn. “Constraints Imposed by CP Conservation in the Presence of Instantons”. In: *Phys. Rev. D* 16 (1977), pp. 1791–1797. DOI: 10.1103/PhysRevD.16.1791.
- [15] Steven Weinberg. “A New Light Boson?” In: *Phys. Rev. Lett.* 40 (1978), pp. 223–226. DOI: 10.1103/PhysRevLett.40.223.
- [16] Frank Wilczek. “Problem of Strong P and T Invariance in the Presence of Instantons”. In: *Phys. Rev. Lett.* 40 (1978), pp. 279–282. DOI: 10.1103/PhysRevLett.40.279.

[17] James D. Bjorken et al. “New Fixed-Target Experiments to Search for Dark Gauge Forces”. In: *Phys. Rev. D* 80 (2009), p. 075018. DOI: [10.1103/PhysRevD.80.075018](https://doi.org/10.1103/PhysRevD.80.075018). arXiv: [0906.0580 \[hep-ph\]](https://arxiv.org/abs/0906.0580).

[18] Philip Ilten et al. “Serendipity in dark photon searches”. In: *JHEP* 06 (2018), p. 004. DOI: [10.1007/JHEP06\(2018\)004](https://doi.org/10.1007/JHEP06(2018)004). arXiv: [1801.04847 \[hep-ph\]](https://arxiv.org/abs/1801.04847).

[19] Martin Bauer, Patrick Foldenauer, and Joerg Jaeckel. “Hunting All the Hidden Photons”. In: *JHEP* 07 (2018), p. 094. DOI: [10.1007/JHEP07\(2018\)094](https://doi.org/10.1007/JHEP07(2018)094). arXiv: [1803.05466 \[hep-ph\]](https://arxiv.org/abs/1803.05466).

[20] Emilie Bertholet et al. “Heavy QCD axion at Belle II: Displaced and prompt signals”. In: *Phys. Rev. D* 105.7 (2022), p. L071701. DOI: [10.1103/PhysRevD.105.L071701](https://doi.org/10.1103/PhysRevD.105.L071701). arXiv: [2108.10331 \[hep-ph\]](https://arxiv.org/abs/2108.10331).

[21] Torben Ferber, Camilo Garcia-Cely, and Kai Schmidt-Hoberg. “BelleII sensitivity to long-lived dark photons”. In: *Phys. Lett. B* 833 (2022), p. 137373. DOI: [10.1016/j.physletb.2022.137373](https://doi.org/10.1016/j.physletb.2022.137373). arXiv: [2202.03452 \[hep-ph\]](https://arxiv.org/abs/2202.03452).

[22] Iftah Galon, David Shih, and Isaac R. Wang. “Dark photons and displaced vertices at the MUonE experiment”. In: *Phys. Rev. D* 107.9 (2023), p. 095003. DOI: [10.1103/PhysRevD.107.095003](https://doi.org/10.1103/PhysRevD.107.095003). arXiv: [2202.08843 \[hep-ph\]](https://arxiv.org/abs/2202.08843).

[23] Triporno Bandyopadhyay, Sabyasachi Chakraborty, and Sokratis Trifinopoulos. “Displaced searches for light vector bosons at Belle II”. In: *JHEP* 05 (2022), p. 141. DOI: [10.1007/JHEP05\(2022\)141](https://doi.org/10.1007/JHEP05(2022)141). arXiv: [2203.03280 \[hep-ph\]](https://arxiv.org/abs/2203.03280).

[24] Joerg Jaeckel and Anh Vu Phan. “Searching dark photons using displaced vertices at Belle II — with backgrounds”. In: *JHEP* 08 (2024), p. 062. DOI: [10.1007/JHEP08\(2024\)062](https://doi.org/10.1007/JHEP08(2024)062). arXiv: [2312.12522 \[hep-ph\]](https://arxiv.org/abs/2312.12522).

[25] Duncan Rocha and Isaac R. Wang. “Filling the Gap: Hunting for Vector Bosons at the MUonE Experiment with Displaced Decay Signature”. In: (Nov. 2025). arXiv: [2511.03222 \[hep-ph\]](https://arxiv.org/abs/2511.03222).

[26] A. Vitez et al. “Anomalous internal pair creation in Be-8 as a signature of the decay of a new particle”. In: *Acta Phys. Polon. B* 39 (2008). Ed. by Marek Pfutzner and Tomasz Matulewicz, pp. 483–488.

[27] A. J. Krasznahorkay et al. “Observation of Anomalous Internal Pair Creation in Be8 : A Possible Indication of a Light, Neutral Boson”. In: *Phys. Rev. Lett.* 116.4 (2016), p. 042501. DOI: [10.1103/PhysRevLett.116.042501](https://doi.org/10.1103/PhysRevLett.116.042501). arXiv: [1504.01527 \[nucl-ex\]](https://arxiv.org/abs/1504.01527).

[28] A. J. Krasznahorkay et al. “New results on the Be-8 anomaly”. In: *PoS BORMIO2017* (2017). Ed. by Laura Fabbietti, Concettina Sfienti, and Wolfgang Kühn, p. 036. DOI: [10.22323/1.302.0036](https://doi.org/10.22323/1.302.0036).

[29] A. J. Krasznahorkay et al. “New anomaly observed in He4 supports the existence of the hypothetical X17 particle”. In: *Phys. Rev. C* 104.4 (2021), p. 044003. DOI: [10.1103/PhysRevC.104.044003](https://doi.org/10.1103/PhysRevC.104.044003). arXiv: [2104.10075 \[nucl-ex\]](https://arxiv.org/abs/2104.10075).

[30] A. J. Krasznahorkay et al. “New anomaly observed in C12 supports the existence and the vector character of the hypothetical X17 boson”. In: *Phys. Rev. C* 106.6 (2022), p. L061601. DOI: [10.1103/PhysRevC.106.L061601](https://doi.org/10.1103/PhysRevC.106.L061601). arXiv: [2209.10795 \[nucl-ex\]](https://arxiv.org/abs/2209.10795).

[31] A. J. Krasznahorky et al. “An Update of the Hypothetical X17 Particle”. In: *Universe* 10.11 (2024), p. 409. DOI: [10.3390/universe10110409](https://doi.org/10.3390/universe10110409). arXiv: [2409.16300 \[nucl-ex\]](https://arxiv.org/abs/2409.16300).

[32] F. W. N. de Boer et al. “A deviation in internal pair conversion”. In: *Phys. Lett. B* 388 (1996), pp. 235–240. DOI: [10.1016/S0370-2693\(96\)01311-1](https://doi.org/10.1016/S0370-2693(96)01311-1).

[33] F. W. N. de Boer et al. “Excess in e+ e- pairs near 9 MeV/c^2 invariant mass”. In: *J. Phys. G* 23 (1997), pp. L85–L96. DOI: [10.1088/0954-3899/23/11/001](https://doi.org/10.1088/0954-3899/23/11/001).

[34] F. W. N. de Boer et al. “Further search for a neutral boson with a mass around 9-MeV/c**2”. In: *J. Phys. G* 27 (2001), p. L29. DOI: [10.1088/0954-3899/27/4/102](https://doi.org/10.1088/0954-3899/27/4/102). arXiv: [hep-ph/0101298](https://arxiv.org/abs/hep-ph/0101298).

[35] A. Krasznahorkay et al. “Lepton pairs from a forbidden M0 transition: Signaling an elusive light neutral boson?” In: *Acta Phys. Polon. B* 37 (2006). Ed. by T. Matulewicz and Z. Sujkowski, pp. 239–244.

[36] Jonathan L. Feng et al. “Particle physics models for the 17 MeV anomaly in beryllium nuclear decays”. In: *Phys. Rev. D* 95.3 (2017), p. 035017. DOI: [10.1103/PhysRevD.95.035017](https://doi.org/10.1103/PhysRevD.95.035017). arXiv: [1608.03591 \[hep-ph\]](https://arxiv.org/abs/1608.03591).

[37] Jonathan L. Feng, Tim M. P. Tait, and Christopher B. Verhaaren. “Dynamical Evidence For a Fifth Force Explanation of the ATOMKI Nuclear Anomalies”. In: *Phys. Rev. D* 102.3 (2020), p. 036016. DOI: [10.1103/PhysRevD.102.036016](https://doi.org/10.1103/PhysRevD.102.036016). arXiv: [2006.01151 \[hep-ph\]](https://arxiv.org/abs/2006.01151).

[38] Jonathan Kozaczuk, David E. Morrissey, and S. R. Stroberg. “Light axial vector bosons, nuclear transitions, and the ${}^8\text{Be}$ anomaly”. In: *Phys. Rev. D* 95.11 (2017), p. 115024. DOI: [10.1103/PhysRevD.95.115024](https://doi.org/10.1103/PhysRevD.95.115024). arXiv: [1612.01525 \[hep-ph\]](https://arxiv.org/abs/1612.01525).

[39] Daniele Barducci and Claudio Toni. “An updated view on the ATOMKI nuclear anomalies”. In: *JHEP* 02 (2023). [Erratum: *JHEP* 07, 168 (2023)], p. 154. DOI: [10.1007/JHEP02\(2023\)154](https://doi.org/10.1007/JHEP02(2023)154). arXiv: [2212.06453 \[hep-ph\]](https://arxiv.org/abs/2212.06453).

[40] M. Achasov et al. “STCF conceptual design report (Volume 1): Physics & detector”. In: *Front. Phys. (Beijing)* 19.1 (2024), p. 14701. DOI: [10.1007/s11467-023-1333-z](https://doi.org/10.1007/s11467-023-1333-z). arXiv: [2303.15790 \[hep-ex\]](https://arxiv.org/abs/2303.15790).

[41] Jiancong Bao et al. “Conceptual Design Report of Super Tau-Charm Facility: The Accelerator”. In: (Sept. 2025). arXiv: [2509.11522 \[physics.acc-ph\]](https://arxiv.org/abs/2509.11522).

[42] Emilie Bertholet and Abner Soffer. “Estimating the track-reconstruction efficiency in phenomenological proposals of long-lived-particle searches”. In: *Int. J. Mod. Phys. A* 40.15 (2025), p. 2550032. DOI: [10.1142/S0217751X25500320](https://doi.org/10.1142/S0217751X25500320). arXiv: [2501.00857 \[hep-ex\]](https://arxiv.org/abs/2501.00857).

[43] S. Agostinelli et al. “GEANT4 - A Simulation Toolkit”. In: *Nucl. Instrum. Meth. A* 506 (2003), pp. 250–303. DOI: [10.1016/S0168-9002\(03\)01368-8](https://doi.org/10.1016/S0168-9002(03)01368-8).

[44] M. E. Rose. “Internal Pair Formation”. In: *Phys. Rev.* 76 (1949). [Erratum: *Phys. Rev.* 78, 184–184 (1950)], pp. 678–681. DOI: [10.1103/PhysRev.78.184](https://doi.org/10.1103/PhysRev.78.184).

[45] M. E. Rose. “Internal Pairs from Aligned Nuclei”. In: *Phys. Rev.* 131 (1963), pp. 1260–1264. DOI: [10.1103/PhysRev.131.1260](https://doi.org/10.1103/PhysRev.131.1260).

[46] E. K. Warburton. “Internal Pair Emission from Aligned Nuclei”. In: *Phys. Rev.* 133 (6B Mar. 1964), B1368–B1372. DOI: [10.1103/PhysRev.133.B1368](https://doi.org/10.1103/PhysRev.133.B1368). URL: <https://link.aps.org/doi/10.1103/PhysRev.133.B1368>.

[47] A. Borsellino. “Momentum Transfer and Angle of Divergence of Pairs Produced by Photons”. In: *Phys. Rev.* 89 (1953), pp. 1023–1025. DOI: [10.1103/PhysRev.89.1023](https://doi.org/10.1103/PhysRev.89.1023).

[48] E. L. Hart et al. “Electron Pair Production in the Field of the Proton and in the Field of the Electron by Photons of Energy from 10 Mev to 1 Bev”. In: *Phys. Rev.* 115 (1959), pp. 678–686. DOI: [10.1103/PhysRev.115.678](https://doi.org/10.1103/PhysRev.115.678).

[49] Haakon Olsen. “Opening Angles of Electron-Positron Pairs”. In: *Phys. Rev.* 131 (1963), pp. 406–415. DOI: [10.1103/PhysRev.131.406](https://doi.org/10.1103/PhysRev.131.406).

[50] Tran The Anh et al. “Checking the ${}^8\text{Be}$ Anomaly with a Two-Arm Electron Positron Pair Spectrometer”. In: *Universe* 10.4 (2024), p. 168. DOI: [10.3390/universe10040168](https://doi.org/10.3390/universe10040168). arXiv: [2401.11676 \[nucl-ex\]](https://arxiv.org/abs/2401.11676).

[51] Kh. U. Abraamyan et al. “Observation of structures at ~ 17 and ~ 38 MeV/c 2 in the $\gamma\gamma$ invariant mass spectra in pC, dC, and dCu collisions at p_{lab} of a few GeV/c per nucleon”. In: (Nov. 2023). arXiv: 2311.18632 [hep-ex].

[52] Ann-Kathrin Perrevoort. “A Review of $\mu \rightarrow eee$, $\mu \rightarrow e\gamma$ and $\mu N \rightarrow eN$ Conversion”. In: PoS FPCP2023 (2023), p. 015. DOI: 10.22323/1.445.0015. arXiv: 2310.15713 [hep-ex].

[53] G. Azuelos et al. “Status of the X17 search in Montreal”. In: *J. Phys. Conf. Ser.* 2391.1 (2022), p. 012008. DOI: 10.1088/1742-6596/2391/1/012008. arXiv: 2211.11900 [physics.ins-det].

[54] Bastin, Beyhan et al. “Investigation of a light Dark Boson existence: The New JEDI project”. In: *EPJ Web Conf.* 275 (2023), p. 01012. DOI: 10.1051/epjconf/202327501012. URL: <https://doi.org/10.1051/epjconf/202327501012>.

[55] Daniele S. M. Alves et al. “Shedding light on X17: community report”. In: *Eur. Phys. J. C* 83.3 (2023), p. 230. DOI: 10.1140/epjc/s10052-023-11271-x.

[56] Gianpiero Gervino et al. “X17 search project with EAR2 neutron beam”. In: *EPJ Web Conf.* 279 (2023), p. 13007. DOI: 10.1051/epjconf/202327913007.

[57] Martin Sevior et al. “A Time Projection Chamber to Search for Feebly Interacting Bosons via Proton Induced Nuclear Reactions”. In: (Feb. 2023). arXiv: 2302.13281 [hep-ex].

[58] Attila J. Krasznahorkay. “Experiments to Detect the Hypothetical X17 Particle”. In: *Acta Phys. Polon. Supp.* 18.4 (2025), 4–A1. DOI: 10.5506/APhysPolBSupp.18.4-A1.

[59] F. Bossi et al. “Search for a new 17 MeV resonance via e^+e^- annihilation with the PADME Experiment”. In: (May 2025). arXiv: 2505.24797 [hep-ex].

[60] K. Afanaciev et al. “Search for the X17 particle in ${}^7\text{Li}(p, e^+e^-){}^8\text{Be}$ processes with the MEG II detector”. In: *Eur. Phys. J. C* 85.7 (2025), p. 763. DOI: 10.1140/epjc/s10052-025-14345-0. arXiv: 2411.07994 [nucl-ex].

[61] Xilin Zhang and Gerald A. Miller. “Can nuclear physics explain the anomaly observed in the internal pair production in the Beryllium-8 nucleus?” In: *Phys. Lett. B* 773 (2017), pp. 159–165. DOI: 10.1016/j.physletb.2017.08.013. arXiv: 1703.04588 [nucl-th].

[62] Ulrich Ellwanger and Stefano Moretti. “Possible Explanation of the Electron Positron Anomaly at 17 MeV in ${}^8\text{Be}$ Transitions Through a Light Pseudoscalar”. In: *JHEP* 11 (2016), p. 039. DOI: 10.1007/JHEP11(2016)039. arXiv: 1609.01669 [hep-ph].

[63] Luigi Delle Rose, Shaaban Khalil, and Stefano Moretti. “Explanation of the 17 MeV Atomki anomaly in a $U(1)'$ -extended two Higgs doublet model”. In: *Phys. Rev. D* 96.11 (2017), p. 115024. DOI: 10.1103/PhysRevD.96.115024. arXiv: 1704.03436 [hep-ph].

[64] Luigi Delle Rose et al. “Atomki Anomaly in Family-Dependent $U(1)'$ Extension of the Standard Model”. In: *Phys. Rev. D* 99.5 (2019), p. 055022. DOI: 10.1103/PhysRevD.99.055022. arXiv: 1811.07953 [hep-ph].

[65] Triparno Bandyopadhyay. “Dark photons from displaced vertices”. In: *EPJST* 233.11 (Oct. 2024), pp. 2177–2185. ISSN: 1951-6401. DOI: 10.1140/epjs/s11734-024-01087-5. URL: <https://doi.org/10.1140/epjs/s11734-024-01087-5>.

[66] Xiaocong Ai et al. “Design and development of STCF offline software”. In: *Mod. Phys. Lett. A* 39.40 (2024), p. 2440006. DOI: 10.1142/S0217732324400066.

[67] Xiaocong Ai et al. “Performance of Track Reconstruction at STCF Using ACTS”. In: *EPJ Web Conf.* 295 (2024), p. 03029. DOI: 10.1051/epjconf/202429503029.

[68] J. Alwall et al. “The automated computation of tree-level and next-to-leading order differential cross sections, and their matching to parton shower simulations”. In: *JHEP* 07 (2014), p. 079. DOI: 10.1007/JHEP07(2014)079. arXiv: 1405.0301 [hep-ph].

[69] Emilie Bertholet et al. “Searching for long-lived light neutralinos from B -meson decays with baryonic R-parity violation at Belle II”. In: (July 2025). arXiv: 2507.00359 [hep-ph].

[70] T. -P. Li and Y. -Q. Ma. “Analysis methods for results in gamma-ray astronomy”. In: *Astrophys. J.* 272 (1983), pp. 317–324. DOI: 10.1086/161295.

[71] Robert D. Cousins, James T. Linnemann, and Jordan Tucker. “Evaluation of three methods for calculating statistical significance when incorporating a systematic uncertainty into a test of the background-only hypothesis for a Poisson process”. In: *Nucl. Instrum. Meth. A* 595.2 (2008), pp. 480–501. DOI: 10.1016/j.nima.2008.07.086. arXiv: physics/0702156.

[72] Glen Cowan et al. “Asymptotic formulae for likelihood-based tests of new physics”. In: *Eur. Phys. J. C* 71 (2011). [Erratum: Eur.Phys.J.C 73, 2501 (2013)], p. 1554. DOI: 10.1140/epjc/s10052-011-1554-0. arXiv: 1007.1727 [physics.data-an].

[73] Nilanjana Kumar and Stephen P. Martin. “Vectorlike Leptons at the Large Hadron Collider”. In: *Phys. Rev. D* 92.11 (2015), p. 115018. DOI: 10.1103/PhysRevD.92.115018. arXiv: 1510.03456 [hep-ph].

[74] Luca Di Luzio, Paride Paradisi, and Nudzeim Selimovic. “Hunting for a 17 MeV particle coupled to electrons”. In: (Apr. 2025). arXiv: 2504.14014 [hep-ph].

[75] Charles R. Harris et al. “Array programming with NumPy”. In: *Nature* 585.7825 (Sept. 2020), pp. 357–362. DOI: 10.1038/s41586-020-2649-2. URL: <https://doi.org/10.1038/s41586-020-2649-2>.

[76] Pauli Virtanen et al. “SciPy 1.0: Fundamental Algorithms for Scientific Computing in Python”. In: *Nature Methods* 17 (2020), pp. 261–272. DOI: 10.1038/s41592-019-0686-2.

[77] J. D. Hunter. “Matplotlib: A 2D graphics environment”. In: *Computing in Science & Engineering* 9.3 (2007), pp. 90–95. DOI: 10.1109/MCSE.2007.55.

[78] Xiaocong Ai, Xingtao Huang, and Yi Liu. “Implementation of ACTS for STCF track reconstruction”. In: *JINST* 18.07 (2023), P07026. DOI: 10.1088/1748-0221/18/07/P07026. arXiv: 2301.04306 [hep-ex].

[79] Lu-Kui Jia et al. “Study of low momentum track reconstruction for the BESIII main drift chamber”. In: *Chin. Phys. C* 34 (2010), pp. 1866–1873. DOI: 10.1088/1674-1137/34/12/014.

[80] Xiaoqian Jia et al. “BESIII track reconstruction algorithm based on machine learning”. In: *EPJ Web Conf.* 295 (2024), p. 09006. DOI: 10.1051/epjconf/202429509006.

[81] Liang-Liang Wang. “Track Reconstruction at BESIII”. In: (May 2024). Presented at the Workshop on Tracking in Particle Physics Experiments. URL: https://indico.ihep.ac.cn/event/21775/contributions/155274/attachments/78219/97278/20240517_BESIII_Track_reconstruction.pdf.